THE SOCIETY OF NAVAL ARCHITECTS AND MARINE ENGINEERS
and
THE SHIP STRUCTURE COMMITTEE

Paper presented at the Ship Structures Symposium '93
Sheraton National Hotel, Arlington, Virginia, November 16-17, 1993

Applications of Spectral Fatigue Analysis to the ARCO 190 Mdwt Tankers

David Sucharski[1] and Dr. Maxwell C. Cheung, P.E.[2]

[1]Manager of Technical Services, ARCO Marine, Long Beach, California
[2]President, MCA Engineers, Inc., Costa Mesa, California

Abstract

ARCO Marine, Inc. supported by MCA Engineers, Inc. strengthened its response to structural fracturing in its tankers with the development of an analytical procedure for determining the fatigue resistance of critical details. This paper gives a brief summary of some of the causes of fatigue fracturing in the ARCO TAPS tankers, the extent and type of fractures observed and a description of the fatigue analysis procedure and its application to typical details in one class of tanker.

Introduction

Between the late 1960's and early 1980's the TAPS tanker fleet was built to transport Alaskan North Slope crude oil from Valdez, Alaska to the West coast of the United States and Panama. Most of the new ships are part of seven different classes built at four different US shipyards. The largest classes were built in response to the unrealized expectation of cargo preference, but subsequently went into TAPS service. The five ships of the 70,000 dwt Sansinena Class are the smallest and the three ships of the 265,000 dwt Massachusetts Class are the largest. ARCO Marine Inc. (AMI) operates four different classes of TAPS tankers built as part of this program, two ships of the Massachusetts Class, two ships of the 189,000 dwt San Diego Class, three ships of the 120,00 dwt ARCO Anchorage Class, and two ships of the Sansinena Class. By the mid 1980's extensive fracturing was occurring in many of these ships. Within the AMI fleet, anecdotal information suggested that the ships built nearer the end of the TAPS fleet program were experiencing more fractures than ships built earlier. AMI and AeroHydro Inc. developed the AMI hull fracture database (HFDB) which permitted cataloging of all fractures in the cargo block of each AMI tanker by location, severity and type of structure affected. This more organized view confirmed the earlier impression that the more recent ships were more susceptible to fracturing.

Initially the cause of this fracturing problem was not well understood. Two types of fractures occurred, a few fractures across deep members like the underdeck transverse web frames and underdeck girder of the CVK, and many essentially nuisance fractures in the brackets and connections between secondary structure like bulkhead vertical stiffeners and bottom longitudinal. It was not possible to explain the failures with any reasonable load using either simplified beam theory or finite element analysis (FEA). These fractures were clearly occurring at average stresses below the elastic limit of the steel. The most probable cause is fatigue at stress concentration sites at structural connections. This paper briefly addresses some of the causes for the poor fatigue resistance of the TAPS fleet, its impact on the industry, typical examples of the extent of fracturing in two classes of AMI tankers, and a description with examples of the process developed by MCA Engineers Inc., Ocean Systems Inc. and ARCO Marine Inc. to ensure that fatigue in the ARCO ships is managed effectively.

Causes and Effects

Fatigue fracturing in ships is not new. What is new is the intensity and frequency of fatigue fracturing found in the TAPS fleet. This situation developed mainly because there was no process for ensuring fatigue resistant ships during the design of the TAPS tankers. In addition, several factors emerged and intensified during the TAPS fleet building program that increased the probability that fatigue problems would occur.

When the TAPS tankers were designed, there was no practical process in place to assess probable fatigue performance, nor were there explicit fatigue performance criteria. Rigorous analytical tools were not available.

Fatigue was not recognized as a threat to the ships, and typically was not a consideration in the design process. Designers did know that soft transitions between structural elements and continuity are important, but minimizing stress concentrations to ensure a reliable structure was mainly left to intuition and "good marine practice" rather than analysis.

In addition to the lack of adequate analysis technology for avoiding fatigue problems, the situation was further complicated by the rapid increase in ship size, efforts to increase production efficiency, the increasing use of high strength steel, and the unexpectedly severe environment in the North Pacific. Each of these factors had a negative effect on the fatigue resistance of the TAPS fleet that seemed to grow worse with each succeeding class.

During the TAPS fleet buildup, tanker size grew rapidly. Within approximately a decade, the size of tankers went from 40,000 dwt to 265,000 dwt. This rapid increase in ship size pushed the existing technology beyond the limits of reliable performance. Ship design was considerably influenced by empiricism and the repetition of successful past ships. Such a rapid and extreme extrapolation beyond experience was a severe challenge to the design process.

Throughout the design of the TAPS fleet, increasing emphasis was devoted to improved production efficiency. One practical effect was the increasing use of simplified details and thinner scantlings. As a result, some of these tankers are characterized by numerous, repetitive hard spots, and relatively large average stress values. In some cases designers extrapolated beyond experience with a process significantly influenced by experience while simultaneously abandoning proven practices. Startling departures from the known need for good continuity and the avoidance of abrupt structural transitions were too often overlooked and tolerated by both the owner and regulatory authorities.

High strength steel was increasingly used in succeeding classes of TAPS tankers in an effort to reduce steel weight by using thinner sections of a stronger material. Perhaps counter-intuitively, the fatigue resistance of higher strength steels and weldments is not superior to mild steel. The design process seems to have exclusively considered elastic strength with no appreciation for the deterioration of fatigue resistance associated with the resulting higher average stresses. This situation and its probable disruptive effect on the reliability of the structure was not recognized by the owners, designers, and regulators at the time.

The TAPS tankers spend an unusual proportion of their time in stormy seas. The average stress levels in these ships exceeds the expectations of normal experience and is an important contributing factor to the early and severe onset of fatigue. There was no comparable experience operating large tankers in constantly stormy seas for such a lengthy service life. This lack of experience significantly handicapped a design process substantially influenced by empiricism. The hostile environment was exacerbated by a departure from established good seakeeping design in some classes including the lack of forescastles and the use of full hull forms with poor powering and seakeeping in even moderate seas.

The extensive fatigue fracturing in the TAPS fleet has had three effects: reduced fleet efficiency, more regulatory oversight, and improved fatigue analysis. The industry's experience with fatigue fracturing in the TAPS fleet is extensive. It is not unusual to repair more than one hundred fractures in the cargo block of a TAPS tanker at each bi-annual shipyard period. Occasionally fractures occur between shipyard periods necessitating both expensive repairs and extensive lost revenue while the ship is tank cleaning an undergoing the repair. In 1992, the USCG implemented the Critical Area Inspection Plan process for TAP tankers in response to the extensive fracturing reported in the fleet. This process requires an inspection of the structure of each tank in the cargo block every year. Based on the ship's history, close up inspections may be required in some locations necessitating expensive staging. Typically cleaning the ship, making the inspection (plus any repairs needed) removes the ship from service for seven to ten days. This situation is certainly an unexpected and unintended consequence of building a fleet of large tankers to move oil from Alaska to the US West coast.

The most positive result of the fracturing is the incentive it gave for developing analytical tools that ensure fatigue resistant designs and repairs. Recognizing the long term prospect of increasing fatigue problems as the ships age, AMI initiated a program in 1989 to better manage and minimize fracturing in its fleet. Initially the work focused on better documentation of fractures through the creation and use of Hull Fracture Data Base (HFDB). HFDB catalogs all fractures in the cargobox section of the AMI tankers by ship, class, date of discovery, location, severity, and type of structure affected. Figures 1 and 2 show typical output from the database for the AMI 190,000 dwt tankers. These figures are composites showing the transverse and vertical distribution (Figure 1), and the longitudinal distribution (Figure 2) of all of the fractures reported. Figure 1 shows that most fractures occur at the structural connections along the boundaries of the shell, inner bottom and transverse webs and bulkheads. Figure 2 shows that the aft boundaries of wing ballast tanks, and cargo tanks routinely used for storm ballast are also important sites for fracturing. These results focus AMI's inspection and repair resources to systematically monitor and eliminate fracture prone details. For example, deeper access to

HFDB reveals that most of the fractures shown along the sideshell in Figure 1 occur in the connection between the sideshell longitudinal and the flatbar tie plate connecting them to the outermost vertical stiffener on transverse bulkheads. This type of fracture is particularly troublesome because occasionally it spreads across the longitudinal into the sideshell. In that case the oil water boundary is perforated and immediate repairs are necessary. AMI supported by MCA redesigned this connection and modified the structure to eliminate this problem detail.

Figures 3 and 4 show the transverse/vertical and longitudinal distribution of fractures in the AMI 120,000 dwt tankers comparable to Figures 1 and 2 for the AMI 190,000 dwt tankers. These ships are approximately one and a half times older than the 190,000 dwt ships, and were designed near the beginning rather than the end of the TAPS fleet program. The figures show that the distribution of fractures is similar for both classes of ships. For example the 120,000 dwt ships have experienced widespread fracturing at the connections between the bottom longitudinal and vertical stiffeners on transverse bulkheads. HFDB shows that this problem is particularly severe at the aft end of tanks which routinely carry ballast. AMI modified the structure at the most troublesome sites and continues to monitor the integrity of the new connections. Fractures also occur in the 120,000 dwt ships at the connections between sideshell longitudinal and flatbar tieplates at the web frames and transverse bulkheads. Occasionally these fractures have spread to the sideshell.

Once HFDB identified the common fracture sites, elastic analysis was applied to develop design modifications. It was soon discovered that many of the fractures could not be predicted with any plausible load even using FEA and accounting for stress concentrations. The best that could be done was to develop designs with significantly reduced stresses, but the acceptable stress level remained unknown. It became evident that the probable cause of these failures was not elastic overstress, but fatigue at relatively modest stress levels. Clearly an improved analysis that properly accounted for the effects of fatigue, especially as they affected the reliability of connections, was needed. AMI received further incentive to develop a means of assessing fatigue effects in 1991 when studies were initiated to determine the practicality of rebuilding its 120,000 dwt ships with a new inner hull to comply with OPA 90. In particular AMI was concerned about the fatigue life remaining in the existing structure, and how that life might be affected by changes in global stress distribution that could result from the new inner hull. AMI contracted with MCA and OSI for the development of a generalized method for fatigue analysis and its application to the rebuilding design work for the 120,000 dwt class. Subsequently the method has been applied to the ARCO 190,000 dwt and 90,000 dwt tankers, and is an essential part of the repair modification process applied to correct fractures in the AMI fleet. In addition, this method will play a controlling role in the structural design of future ships for the AMI fleet.

Approach

Under a controlled laboratory environment, results of fatigue testing often exhibit large scattering patterns indicating that the fatigue behavior is sensitive to a large number of parameters. Structures operating in the ocean environment in which wind and waves are random, can expect even more scattered results. A standard comprehensive fatigue analytical procedure should be primarily focused on major factors such as: how the ship is built, the distribution of the cargo/ballast and the environment experienced by the ship.

The first factor is pure geometry. Once the ship is built, the stress concentration at the hot spots are inherited and can be calculated accurately by the FEA. Throughout the service life of the tanker, it carries a different amount of liquid cargo/ballast at different tanks and travels different wave climates along the route. Each of these configurations trigger different stress patterns at the hot spots and again can be accurately determined by the FEA.

Utilizing the linear superposition characteristics of these hot spot stresses, a modularized statistical approach is used to calculate the fatigue life of the structural details. The modularize concept enables us to distinguish the consumption of the fatigue life in a specific zone on a specific month. The entire fatigue analysis procedure is summarized by Figure 5.

Trade Route

From Alaska to Panama, the near coastal waters of the Pacific Ocean is divided into 12 zones (Figure 6). For example, the ballast trip from Panama to Valdez traverses every zone except zones 7 and 8. The loaded passage from Valdez to Long Beach goes through zones 6 to 1, ... etc. The weather and movement data are characterized by these zones.

Monthly Zone Sea-Spectra

The short-term sea-states in each of these twelve zones are described by their respective monthly average sea spectrum. A typical example of the month of November in Zone 6 is shown in Figure 7. The mean spectral energies of each wave height group is expressed as a function of the wave periods and wave heights. Although the probability of occurrence of the three smallest wave groups represents more than 83 percent of the records, the energy is low because of the smaller size. On the other hand, the largest wave occurs infrequently and the energy is also low. In most of the records, the energy spectrum of the

higher wave height group shows double peaks indicating that predominant sea and swell exists simultaneously.

Monthly Average Ship Speed

Average ship speed can be compiled with actual historical data or assumed values for design purposes. The ship speed is used to modify the stress RAO to account for the encountering frequencies.

Stress Range RAO

The hot-spot stress of the structural detail is computed by the FEA. In order to realistically simulate the tanker's structural responses to the wave requires a model of the hull that is as large a part as possible. At the same time, fine meshes in the order of inches are required to accurately pin point the hot spot. These contradicting requirements call for using a telescoping technique which models the hull in several stages. The first model provides the largest coverage called "Global Model." The last stage is the "Local Model" with any number of "Intermediate Models" to provide proper transition. In each of these stages, the applied loads must be balanced to achieve static equilibrium.

Global Model

Figure 8 shows a typical Global Model with the shell plating removed for clarity. The model contains the midship cargo block which spans more than two sets of tanks separated by the OT BHD 43, 53 and 62.

The loads applied to this model include steel weight, cargo/ballast, wave pressure and end forces at Frames 41 and 65. For example, Figure 9 shows the distribution of load along the length of the ship when the 190,000 dwt tanker is fully loaded. The highest intensity is about 300 LT/ft. When the ship is subjected to hog wave, as shown in Figure 10, the shear and moment along the length of the ship can be calculated by iterating on the draft, trim and roll until equilibrium is achieved. The shears and moments at Frames 41 and 65 can be interpreted from this calculation and then applied to the Global Model as end forces.

When the Global Model is in perfect equilibrium, no displacement boundary conditions are required. Nevertheless, some soft springs are attached to the model at strategic positions to avoid rigid body motion due to very small load truncation errors.

Intermediate Model

Figure 11 illustrates a typical Intermediate Model with shell plating removed for clarity. Although many structural details, such as stiffeners, are added in this stage of modeling, it is still considered not fine enough to resolve hot-spot characteristics. The purpose of this stage is to provide smoother force transition from the Global to Local Models.

The Intermediate Model can be considered as a free body removed from the Global Model. Along the cut boundaries, there is always a corresponding node in the Intermediate Model for every node in the Global Model. The internal forces at these nodes in the Global Model are transferred as external nodal forces for the Intermediate Model. Together with the internal pressure induced by the cargo/ballast and the external pressure exerted by the wave, the applied force system should be in static equilibrium. Again, soft springs are needed to eliminate rigid body motion.

Local Model

A partial view of a typical Local Model is shown in Figure 12. Fine meshes are applied with discretion to the likely hot-spots, such as rat holes, termination points, abrupt transitions ... etc. In some instances, the characteristic length of the element is in the order of a fraction of an inch.

The procedure of load application to the Local Model is identical to that used by the Intermediate Model. In order to generate the range of stress responses required for the fatigue analysis, 15 type of waves with periods matching those shown in Figure 7 are analyzed. The waves have the following characteristics:

$$\text{Wave Form} = \text{Sinusoidal}$$

$$\text{Wave Length} = 5.125\ T^2$$

$$\text{Wave Height} = \text{Wave Length} / 20.0$$

A hog wave occurs when the crest of the wave reaches the mid point of the ship, and a Sag wave occurs when the trough of the wave reaches that point. The stress range is the measure of the hot spot principal stress between the hog and sag responses. The stress range has zero value when both the stress responses in the hog and sag conditions are in compression. For the fatigue analysis, the stress range is divided by the wave height to obtain the unit response called the Stress Range RAO (Response Amplitude Operator). A typical SR RAO is shown in Figure 13.

Encountering Frequencies

When the ship is traveling at a certain speed (U) at a certain direction (Q) with respect to the dominant wave, its perspective with the ambient wave frequency is changed. In the following fatigue analysis, which requires multiplying the wave energy spectra with the stress range RAO, one of these two parameters must be adjusted with the ship' velocity by using the following formula:

$$W_c = W - \frac{W^2\, U \cos(Q)}{g}$$

where:

W_c = Encountering Frequency

W = Actual Wave Frequency

g = Gravitational Constant

For convenience, the stress range RAOs are mapped to the Encountering Frequency space as shown in Figure 13 for the head and follow sea correction.

S-N Curves

Figure 14 shows a series of S-N curves published by the Department of Energy from the UK and the American Bureau of shipping in the United States. Some curves are assigned for simple geometry with no welding (B and C). Others are for complex shapes with weldment aligned with various orientation from the direction of loading. Each curve is supposed to take into consideration the stress concentration due to geometry, as well as the welding. These curves may be important for preliminary design so that the designer can select a detail based on comparative merits. After the design is made, the stress concentration can be readily computed analytically. The application of these curves must be used with caution.

In fact, many FEA models predict SCF to be in the range of 1.2 to 2.5 depending upon the degree of complexity of the structure. By examining Figure 14, one can have some idea on how much SCF varies from curve to curve. For example, if the structures have the same life span (say one million cycles), the following relative SCF can be derived based on curve D as a reference:

Curve	D	E	F	F2	G	W
SCF	1.000	1.128	1.325	1.514	1.828	2.120

This kind of SCF falls in the range predicted by the FEA. In the following fatigue analysis, curves C or D are used in conjunction with the calculated SCF by the FEA. For numerical computation, the following formula is used:

$$n = a\left\{\left[1 - \left(\frac{S_m}{S_u}\right)^2\right] S_r\right\}^{-B} \quad \text{if } s_m > 0$$

$$n = a\left\{\left[1 + \left(\frac{S_m}{S_u}\right)^2\right] S_r\right\}^{-B} \quad \text{if } s_m < 0$$

where:

N = Number of cycles to failure

A & B are material constants

S_m = Mean Stress

S_u = Ultimate Stress

S_r = Actual Stress Range

Monthly Zone CDR

Once the Stress Range RAO and the Wave Energy Spectra are available, the Response Spectra are calculated month by month and zone by zone with the appropriate Energy Spectra E(W):

$$M_0 = \text{SUM}[\text{RAO}(W, Q)^2 \times E(W)]$$

$$M_2 = \text{SUM}[W^2 \times \text{RAO}(W, Q)^2 \times E(W)]$$

$$M_4 = \text{SUM}[W^4 \times \text{RAO}(W, Q)^2 \times E(W)]$$

where:

M are the spectral moments functions of headings (Q) and cargo/ballast conditions

RAO is a function of frequencies (W), headings (Q) and cargo/ballast conditions

SUM implies summing over entire range of frequencies.

The period of the apparent cycle is assumed to be the zero crossing period which is calculated by:

$$T_2 = 2\pi \sqrt{\frac{M_0}{M_2}} (1 - 0.05\, e)^2$$

where:

$$e = \sqrt{\frac{M_2^2}{M_0 / M_4}}$$

The Unit Cumulative Damage Ratio (UCDR) per unit time, which is a function of zone and month, as well as ships heading and cargo/ballast conditions, are computed as:

$$UCDR = (8M_0)^{B/2}\ \Gamma(1 + B/2)/A/T_2$$

where:

Γ means GAMMA function of ...

For each zone at a specific month, the wave spectra assigns a certain probability for the wave height group (P_k) and the heading (P_j). Modifying U_{CDR} with these probabilities will give the Zone Cumulative Damage Ratio (ZCDR).

$$ZCDR = \text{SUM}\{\text{SUM}[P_k \times P_j \times UCDR]\}$$

Total CDR

The Z_{CDR} is the basic building block of the fatigue analysis. By knowing the ship speed at a certain month, the transit time through a zone can be computed. The Passage

Cumulative Damage Ratio (PCDR) is simply summing the damages through all zones the ship passes.

$$PCDR = SUM [Time \times ZCDR]$$

where:

Time = Transit time through a Zone

SUM implies summing the effect in the Zones the ship passes through

The Total CDR is simply adding the damages sustained by all the trips made since the ship was launched. If the CDR is larger than unity, it means that material fatigue may have occurred earlier.

A typical output is shown in Figure 15 for a particular element on the upper CVK of the 190,000 dwt tanker. Over the 13 years of services, the tanker made 228 round trips between Valdez and Long Beach. It is interesting to note that the damage due to loaded trips is almost double that of the ballast trips. The damage sustained in the winter months (December and January) could be 10 times more severe than the summer months (July and August). The Total CDR is calculated to be 1.363.

Fatigue Life

The Fatigue Life is inversly proportional to the Total CDR. For the sample shown in Figure 15 (Upper CVK), the Fatigue life is:

$$Life = 1 / CDR \times 13 \text{ years}$$

$$= 9.54 \text{ years}$$

More samples for the 190,000 dwt tanker are summarized in Table 1. Four local structural details are investigated:

A. The Side Shell intersects with the transverse oil tight bulkhead and the lowest horizontal stringer. The critical point is at the end of the stringer where it meets with the side shell longitudinal.

B. Upper CVK transition from the vertical member to the longitudinal member. The critical points are the rat hole for the construction joint and the toe of the transition member. These details began failing at approximately the time predicted by the fatigue analysis, and were modified to prevent additioanl failures and ensure an acceptable fatigue life.

C. Lower CVK transition from the vertical member to the inner bottom. Critical points are the upper and lower toes of the transition member.

D. Longitudinal Bulkhead intersects a mid-ship web frame. The critical point is at the stiffener in line with the lower flange of the underdeck web frame. These details began failing at approximately the time predicted by the fatigue analysis and were modified to prevent additional failures and ensure adequate fatigue life.

The original details B and D began failing before the availability of the fatigue analysis. The repair modifications were subsequently analyzed to ensure that an adequate fatigue life was achieved by the repair.

Table 1 also illustrates the effect of the mean stress. For the results reported, it could be noted that when the mean stress is in single digit, the Life expectancy is almost the same as if the mean stress is zero. When the mean stress is between 10 to 20 ksi, the Life expectancy is reduced by a couple of years. However, when the mean stress is high, even when the stress range is low or moderate, the Life expectancy could be reduced appreciably.

Struct. Compnts	Elem. No.	Mean Stress (ksi)			Life (yrs)	
		(1)	(2)	(3)	(4)	(5)
A. Side Shell	1953	13	10	-6	36	34
B. Upper CVK	1609 3234*	12 5	22 0	1 0	18 10	16 10
C. Lower CVK	960 2983	-10 6	10 7	-7 4	38 35	40 34
D.Long Bkhd	3979	6	3	1	15	15
(1) = Winter Ballast						
(2) = Summer Ballast						
(3) = Cargo						
(4) = Ignoring Mean Stress						
(5) = Consider Mean Stress						
* = See Figure 15 for details						

Table 1
Results of Fatigue Analysis of ARCO 190,000 Dwt

Conclusion

The predicted fatigue life from the present analytical procedure is in good agreement with the actual field inspection data for several critical details. The usefulness of this analytical tool was confirmed when the as-built condition and the proposed repair were tested for comparative merit. This saves a great deal of trial and error repairs at the shipyard.

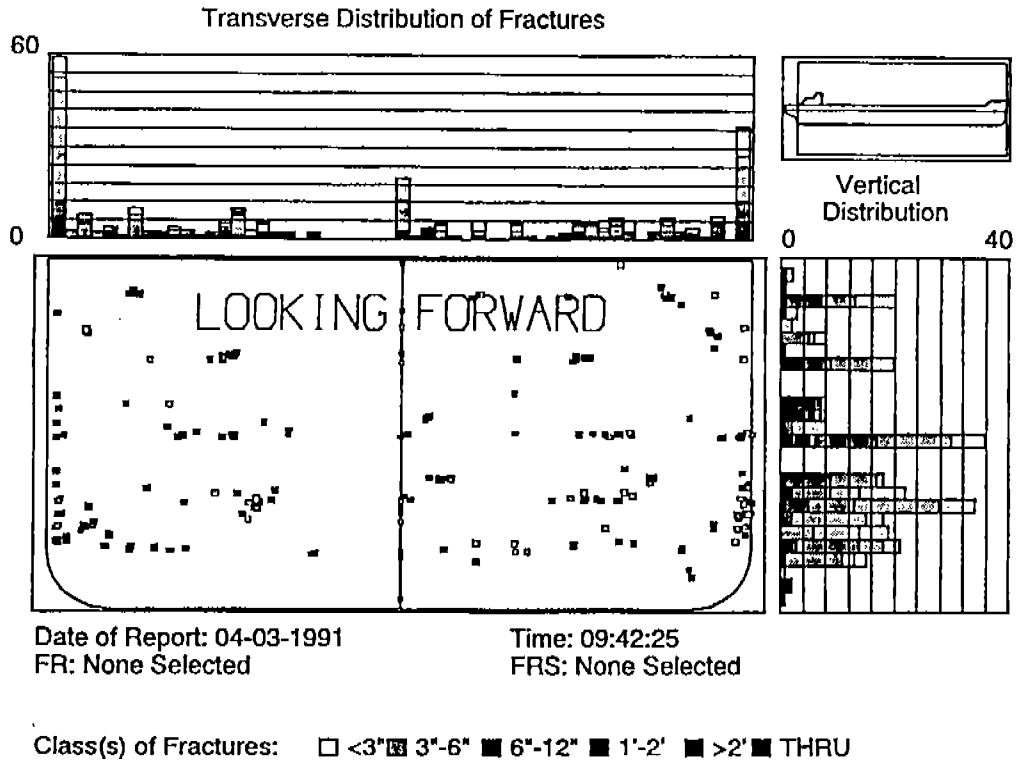

Figure 1
Transverse Distribution of Fractures for the AMI 190,000 DWT Tankers

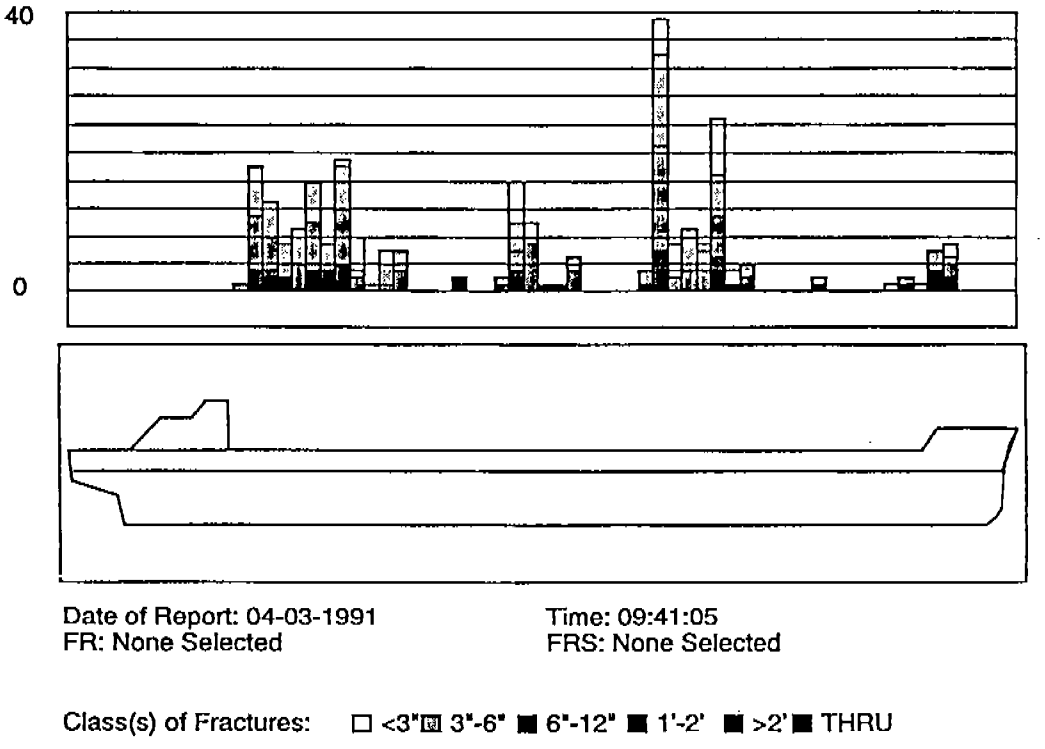

Figure 2
Longitudinal Distribution of Fractures for the AMI 190,000 DWT Tankers

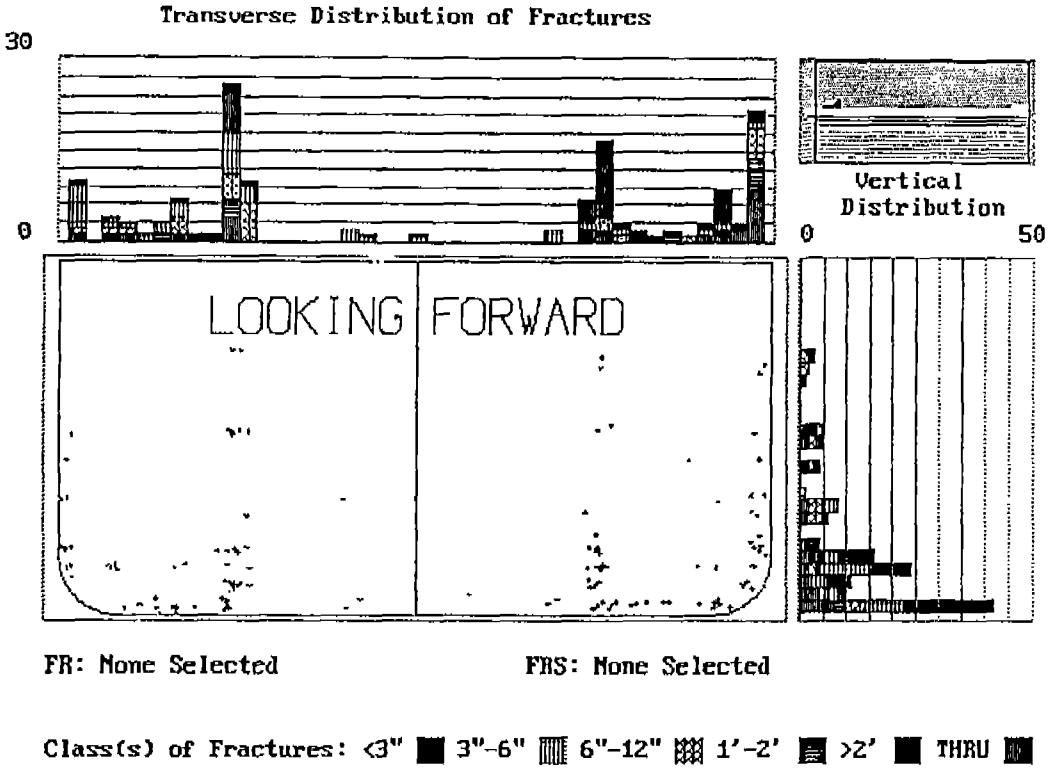

Figure 3
Transverse/Vertical Distribution of Fractures for the AMI 190,000 DWT Tankers

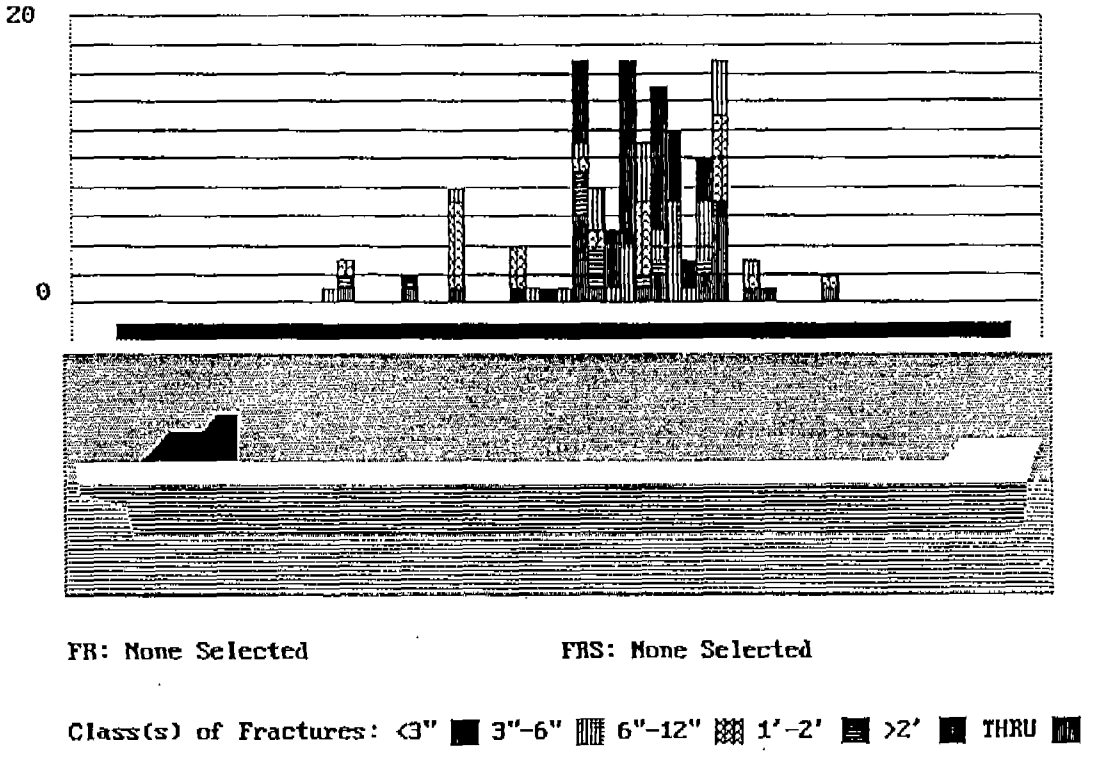

Figure 4
Longitudinal Distribution of Fractures for the AMI 190,000 DWT Tankers

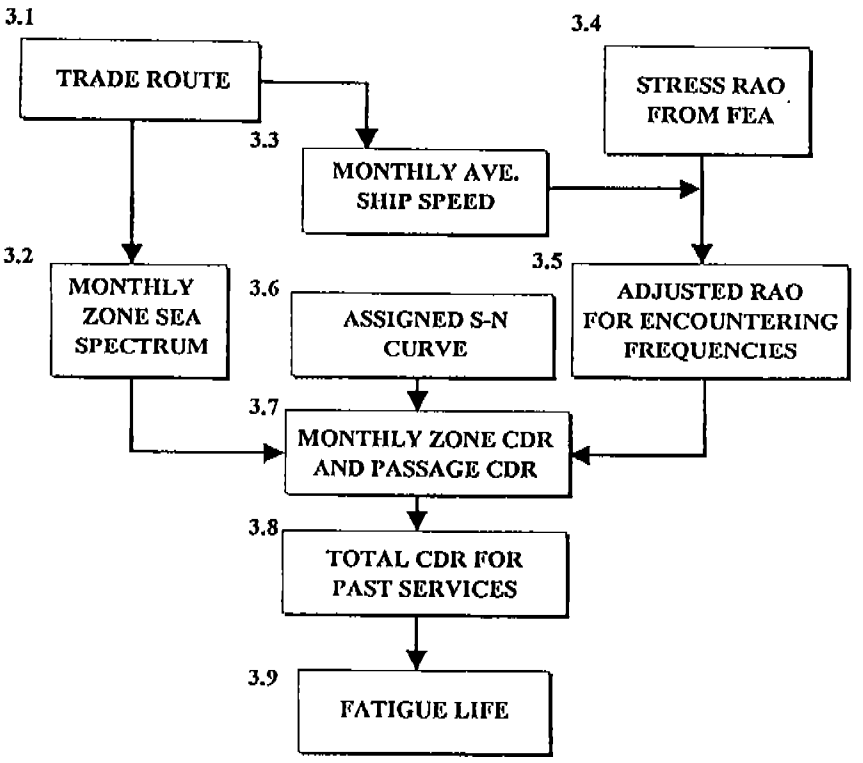

Figure 5
Fatigue Analysis Flow Chart

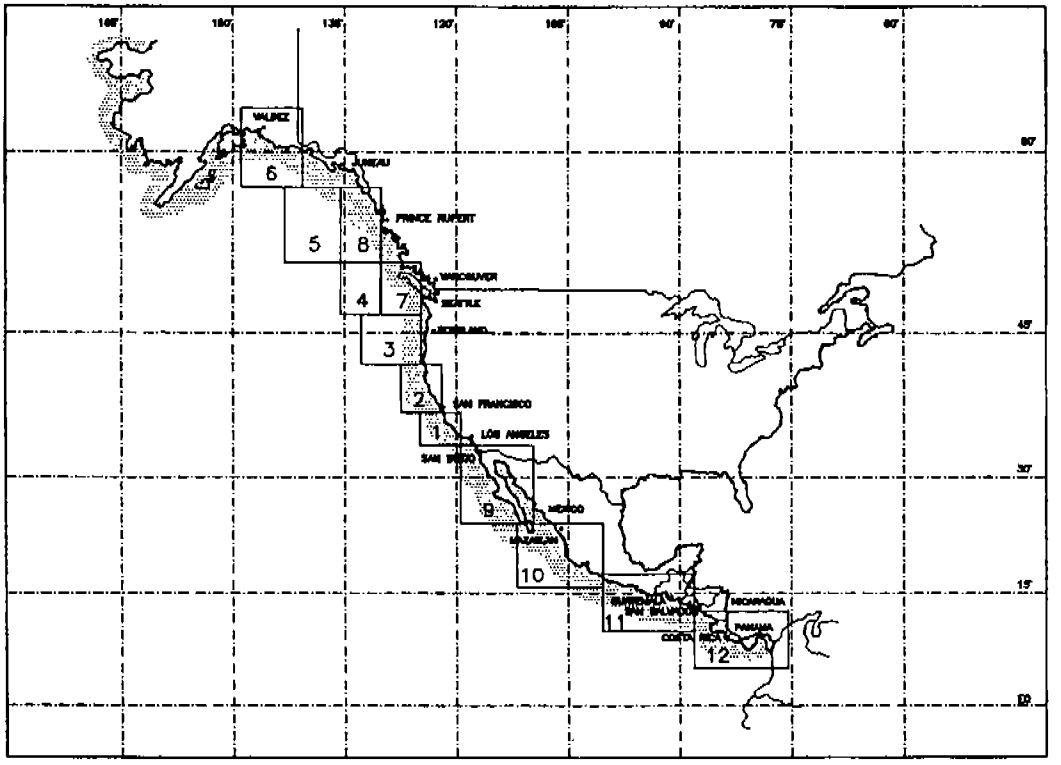

Figure 6
Geographical Zones

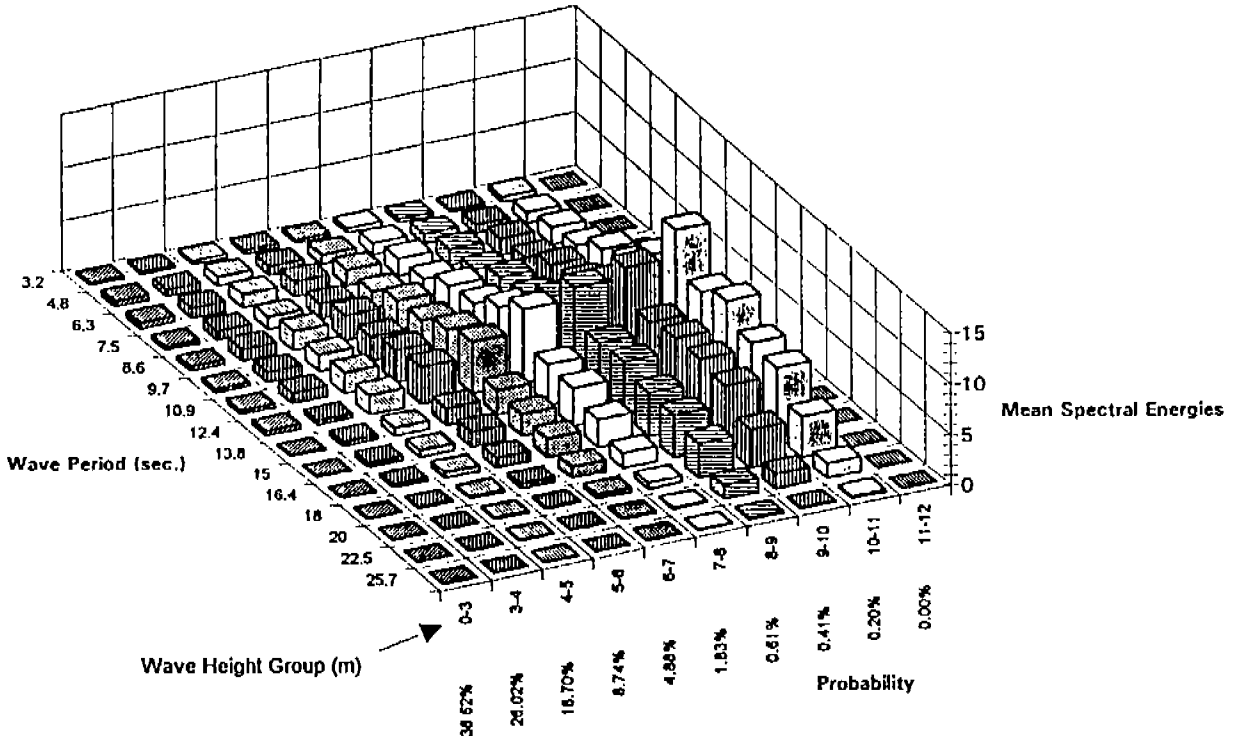

Figure 7
Mean Spectral Energies for Zone 6 (November)

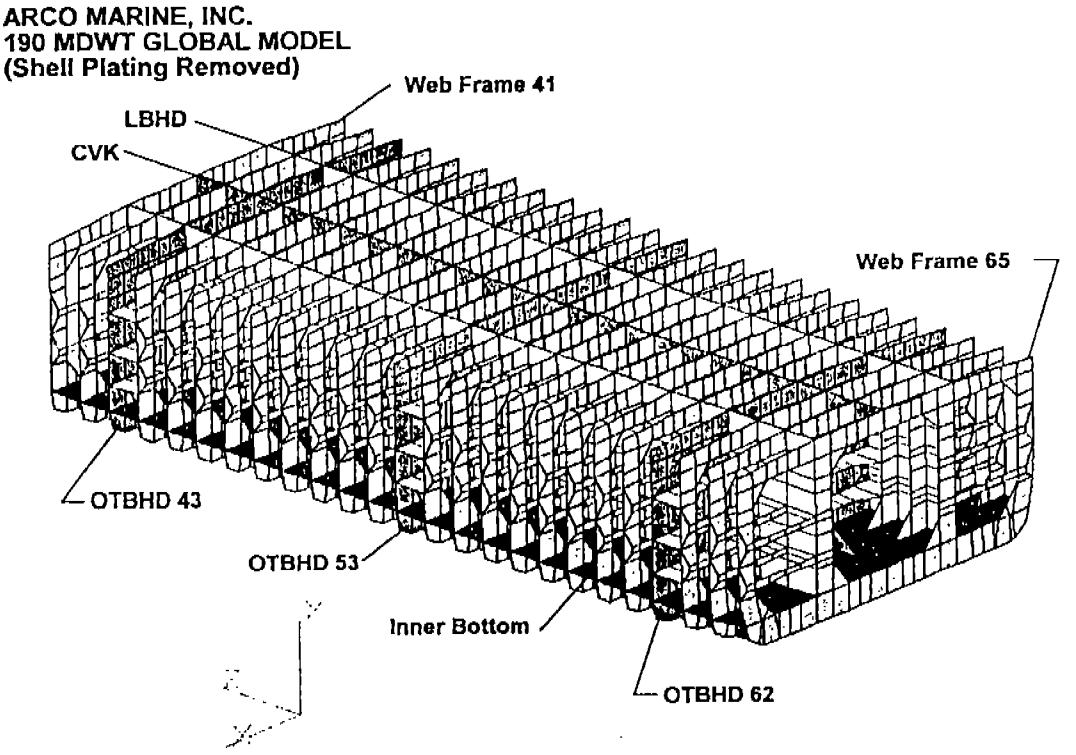

Figure 8
Typical Global Model

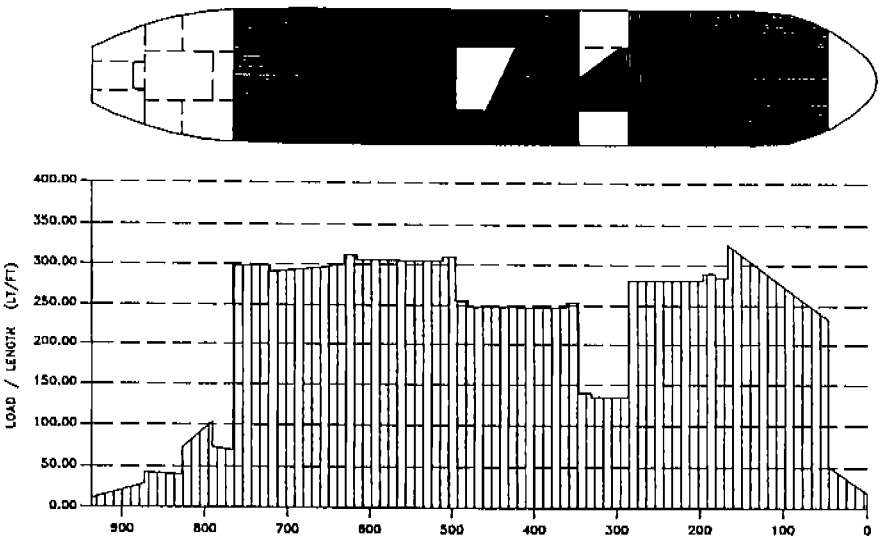

Figure 9
Full Load Distribution

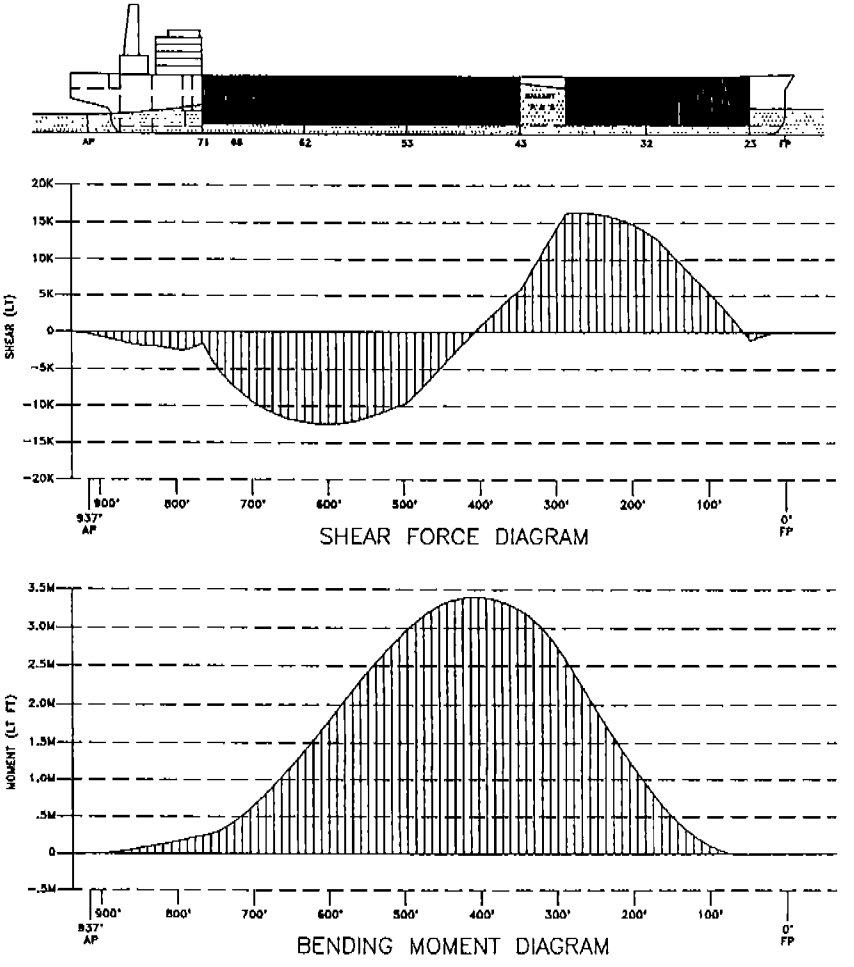

Figure 10
Shear & Moment Distribution @ Hog Wave

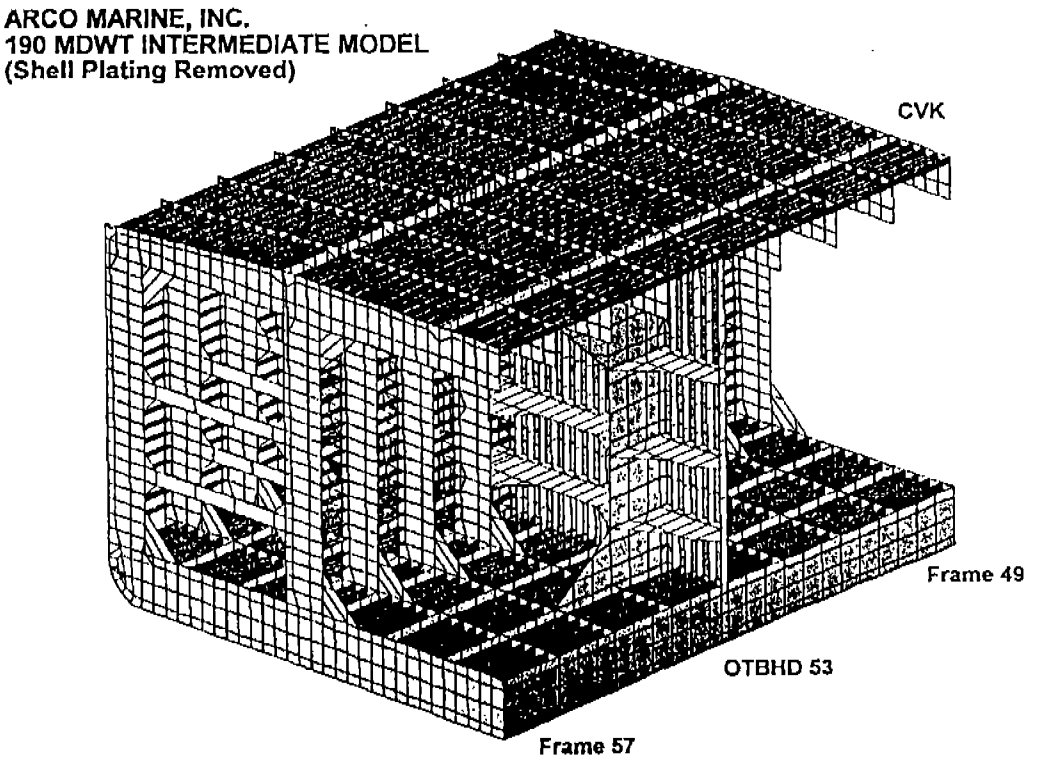

Figure 11
Typical Intermediate Model

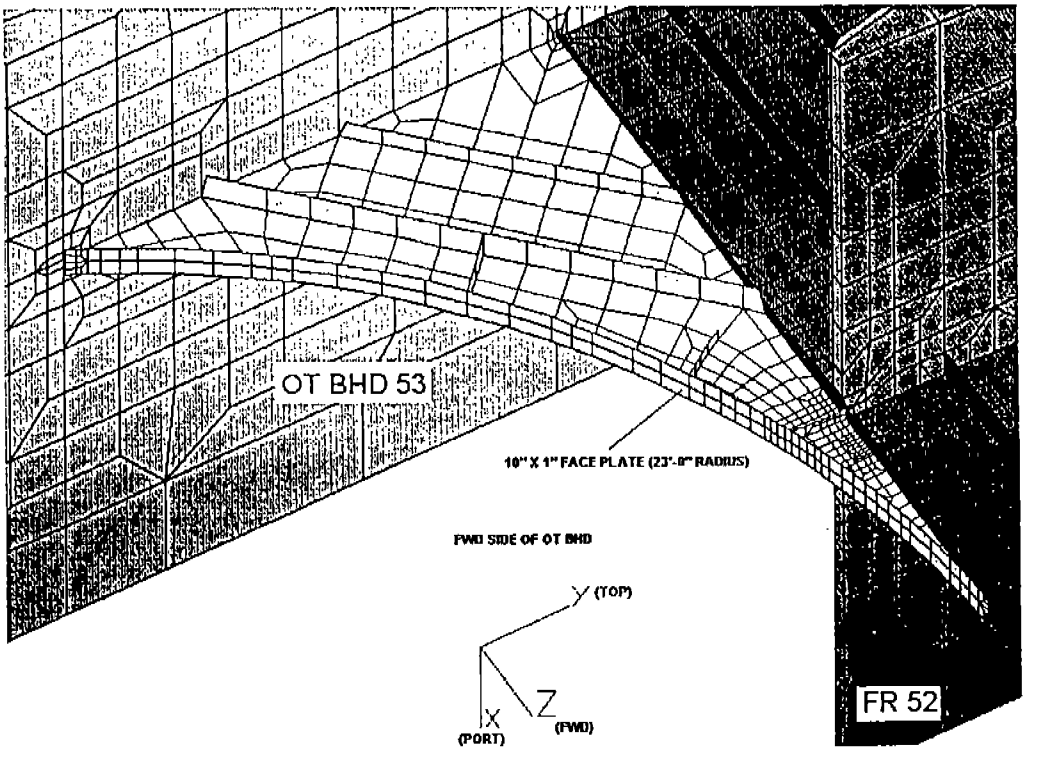

Figure 12
Typical Local Model

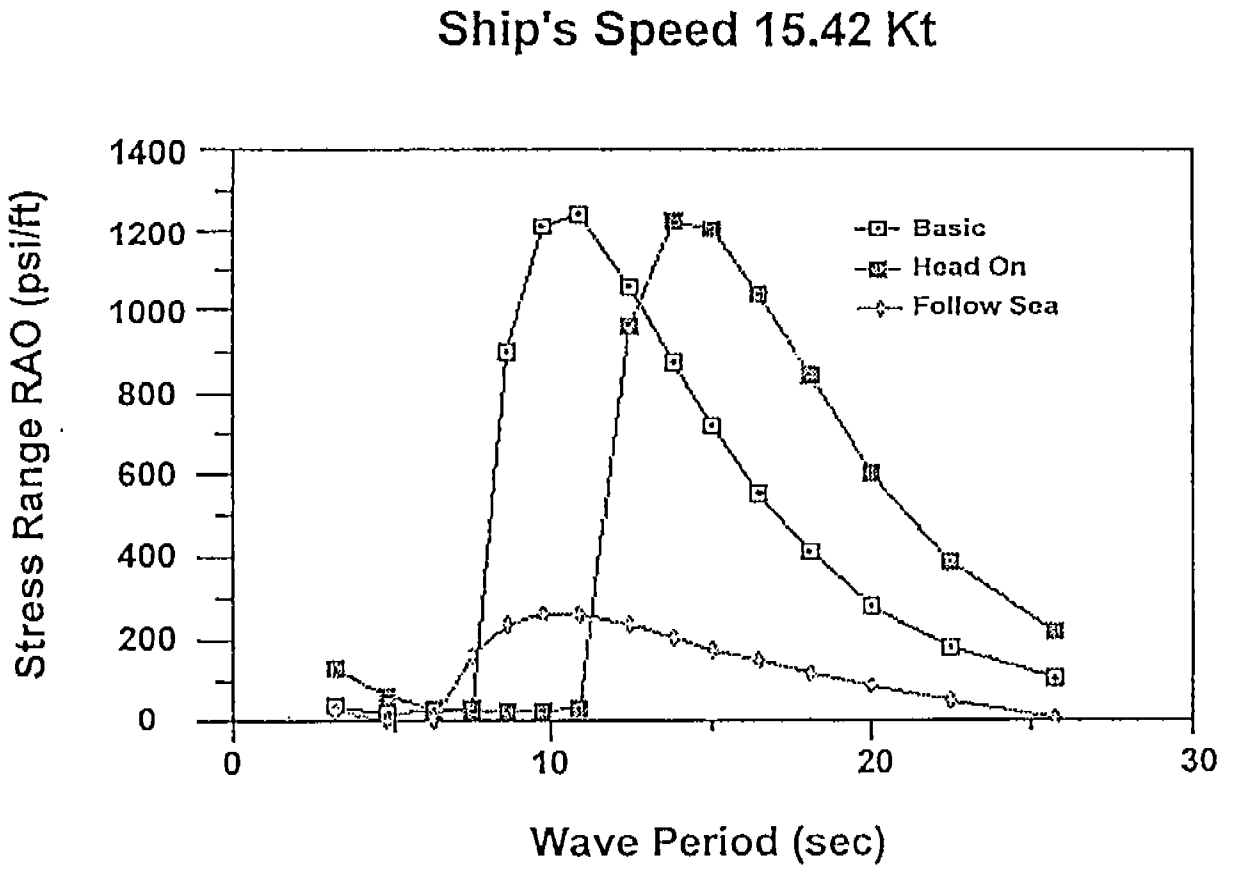

Figure 13
Typical Adjusted Stress Range RAO

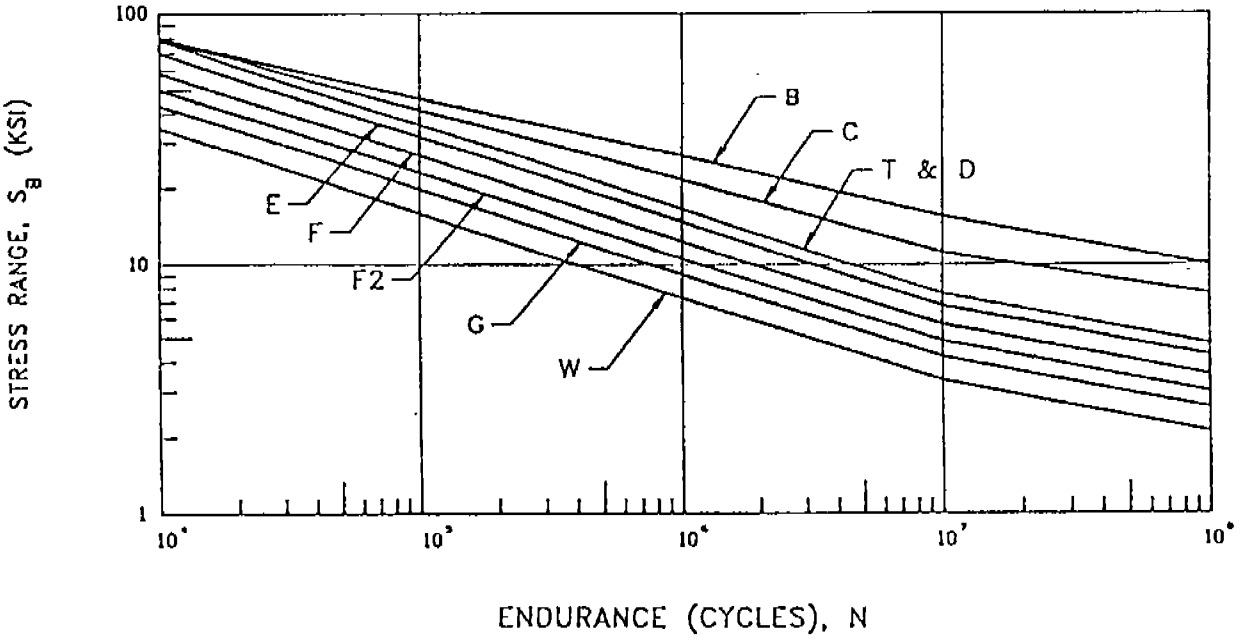

Figure 14
S-N Curves

MODEL: UPPER CVK
ELEMENT: 3234 STRESS: PRINCIPAL STRESS S-N CURVE: D

TABLE FOR MONTHLY CDR CALCULATION

MONTH	VALDEZ TO LONG BEACH			LONG BEACH TO VALDEZ			VALDEZ TO CHERRY POINT			CHERRY POINT TO VALDEZ			LONG BEACH TO SAN FRANCISCO			SAN FRANCISCO TO VALDEZ		
	TRIPS	PCDR	MCDR	TRIPS	PCDR	MCDR	TRIPS	PCDR	MCDR	TRIPS	PCDR	MCDR	TRIPS	PCDR	MCDR	TRIPS	PCDR	MCDR
JAN	21	.0094	.197	24	.0041	.098	0	.0043	.000	0	.0021	.000	1	.0002	.000	1	.0039	.004
FEB	20	.0041	.082	20	.0022	.044	0	.0017	.000	0	.0008	.000	0	.0004	.000	0	.0019	.000
MAR	19	.0038	.072	16	.0026	.042	0	.0014	.000	0	.0010	.000	0	.0003	.000	0	.0017	.000
APR	15	.0032	.048	17	.0019	.032	4	.0016	.006	2	.0011	.002	0	.0002	.000	0	.0015	.000
MAY	16	.0016	.026	15	.0008	.012	3	.0007	.002	4	.0004	.002	0	.0001	.000	0	.0007	.000
JUN	18	.0018	.032	19	.0009	.017	2	.0005	.001	2	.0004	.001	0	.0001	.000	0	.0008	.000
JUL	19	.0011	.021	20	.0003	.006	5	.0002	.001	4	.0001	.000	2	.0003	.001	1	.0002	.000
AUG	21	.0010	.021	18	.0002	.004	6	.0002	.001	6	.0001	.001	1	.0000	.000	2	.0002	.000
SEP	21	.0015	.032	25	.0007	.018	2	.0006	.001	4	.0004	.002	0	.0001	.000	0	.0006	.000
OCT	20	.0022	.044	20	.0013	.026	0	.0010	.000	0	.0006	.000	0	.0001	.000	0	.0010	.000
NOV	16	.0056	.090	16	.0046	.074	0	.0022	.000	1	.0027	.003	0	.0003	.000	0	.0032	.000
DEC	22	.0063	.139	18	.0043	.077	0	.0027	.000	0	.0019	.000	0	.0003	.000	0	.0032	.000
	228		.803	228		.450	22		.013	23		.010	4		.001	4		0.005

MONTH	PORTLAND TO VALDEZ			VALDEZ TO P. ARMUELLES			P. ARMUELLES TO VALDEZ			LONG BEACH TO P. ARMUELLES			P. ARMUELLES TO LONG BEACH		
	TRIPS	PCDR	MCDR	TRIPS	PCDR	MCDR	TRIPS	PCDR	MCDR	TRIPS	PCDR	MCDR	TRIPS	PCDR	MCDR
JAN	0	.0025	.000	2	.0074	.015	0	.0039	.000	0	.0007	.000	1	.0002	.000
FEB	0	.0009	.000	0	.0043	.000	1	.0028	.003	1	.0007	.001	1	.0002	.000
MAR	0	.0011	.000	2	.0040	.008	2	.0025	.005	2	.0008	.002	1	.0003	.000
APR	0	.0013	.000	2	.0029	.006	0	.0020	.000	0	.0004	.000	3	.0001	.000
MAY	0	.0004	.000	2	.0020	.004	0	.0009	.000	1	.0002	.000	0	.0001	.000
JUN	0	.0005	.000	0	.0026	.000	0	.0011	.000	0	.0004	.000	3	.0005	.002
JUL	1	.0001	.000	0	.0019	.000	0	.0005	.000	1	.0005	.001	1	.0001	.000
AUG	1	.0001	.000	0	.0025	.000	0	.0009	.000	0	.0010	.000	0	.0006	.000
SEP	0	.0004	.000	1	.0021	.002	0	.0012	.000	0	.0008	.000	1	.0003	.000
OCT	0	.0006	.000	3	.0038	.011	0	.0016	.000	0	.0007	.000	2	.0002	.000
NOV	1	.0031	.003	2	.0061	.012	0	.0038	.000	0	.0006	.000	1	.0002	.000
DEC	1	.0026	.003	0	.0064	.000	1	.0036	.004	0	.0009	.000	1	.0002	.000
	4		.006	14		.058	4		.011	5		.003	15		.004

TOTAL CDR TO DATE = 1.363

FATIGUE LIFE = 9.54 YRS

TRIPS: TOTAL NO. OF TRIPS DURING 13 YEARS
PCDR: PASSAGE CUMMULATIVE DAMAGE RATIO
MCDR: MONTHLY CUMMULATIVE DAMAGE RATIO

Figure 15
190 MDWT Fatigue Analysis